

Retention and Recycling of Deuterium in Liquid Lithium-Tin Slab Studied by First-Principles Molecular Dynamics

Daye Zheng,^{1,2} Zhen-Xiong Shen,^{1,2} Mohan Chen,^{3,*} Xinguo Ren,^{1,2} and Lixin He^{1,2,†}

¹*Key Laboratory of Quantum Information,
University of Science and Technology of China,
Hefei, Anhui, 230026, People's Republic of China*

²*Synergetic Innovation Center of Quantum Information and Quantum Physics,
University of Science and Technology of China,
Hefei, 230026, People's Republic of China*

³*CAPT, HEDPS, College of Engineering, Peking University,
Beijing 100871, People's Republic of China*

(Dated: September 29, 2020)

Abstract

Understanding the retention and recycling of hydrogen isotopes in liquid metal plasma-facing materials such as liquid Li, Sn, and Li-Sn are of fundamental importance in designing magnetically confined fusion reactors. We perform first-principles molecules dynamics simulations of liquid Li-Sn slab with inserted D atoms to provide microscopic insights into the interactions of D with Li-Sn liquid metal. We prepare two samples with low and high concentrations of D atoms. We observe evaporation of D₂ molecules out of the Li-Sn slabs in both concentrations of D. With detailed analysis, we unveil a cooperative process of forming D₂ molecules in liquid Li-Sn, where Li atoms act as catalytic centers to trap a D atom before another D comes nearby to form a molecule, and the surplus charges are transferred from D₂ to nearby Sn atoms. Furthermore, we predict a temperature window in the low concentration case in which D₂ molecules can escape to vacuum, while LiD molecules cannot. The above findings deepen our understanding of interactions between hydrogen isotopes and Li-Sn liquid metal.

PACS numbers:

I. INTRODUCTION

Plasma-facing components (PFCs) in magnetic confinement fusion devices are designed to withstand high heat loads of bombardments from energetic particles. Meanwhile, hydrogen (H) isotopes such as deuterium (D) and tritium (T) are utilized as fuels and their interactions with PFCs need to be thoroughly understood.¹ In particular, the retention and recycling of D/T attract many attentions due to their impacts on the fueling and vacuum pumping systems, and also the plasma conditions.² Here, *retention* and *recycling* respectively refer to the hydrogen isotopes that remain in PFCs and return back to plasma after the PFCs receive particle bombardments. On one hand, a high retention rate of hydrogen isotopes suggests that the temperature of core plasma is less affected by preventing cold atoms from reentering the plasma, therefore, the plasma performance could be increased with PFCs that can retain a large amount of D/T atoms.³⁻⁵ On the other hand, a high recycling rate of H isotopes can significantly reduce the fuel cost, and a low retention of D/T atoms in PFCs also reduces safety concerns.²

The emergence of liquid-metal PFCs⁶ began receiving widespread attention in recent years. Unlike solid metallic PFCs that unavoidably suffer from mechanical failure problems caused by high energetic particles,⁷⁻⁹ liquid metals for PFCs own a low melting point, resist erosion and neutron damage to a large extent, and has high heat dissipation capabilities. For instance, lithium (Li) has a low melting point of 453 K and was found to improve the plasma parameters in a variety of experiments.^{3-5,10-15} Tin (Sn) has also been tested in several experiments¹⁶⁻¹⁸ due to its low melting point of 505 K,¹⁹ and additionally owns a low vapor pressure that is beneficial for high operating temperatures. Nevertheless, plasma contamination due to accumulation of impurities atoms in plasma is concerned since Sn has a high atomic number. In this regard, Li-Sn eutectic is considered as an alternative candidate for PFCs with combined advantages of both Li and Sn. However, the Li-Sn alloy has been investigated in a few experiments.²⁰⁻²⁴ Therefore, it is of great help to utilize first-principles computational methods to provide fundamental insights into understanding liquid metals²⁵⁻²⁷ and their interactions with hydrogen isotopes.²⁸⁻³¹

Experiments have found that hydrogen isotopes interact differently with liquid Li and liquid Sn. For example, it is known that hydrogen isotopes can be largely absorbed by liquid Li due to their strong chemical affinity with Li atoms.³²⁻³⁵ In contrast, the low reactivity

of Sn with hydrogen isotopes leads to a small retention ratio of hydrogen isotopes in liquid Sn.¹⁸ It is intuitively expected that D atoms can be trapped by Li atoms in liquid Li-Sn eutectic, resulting in a higher number of retained hydrogen isotopes in liquid Li-Sn than liquid Sn. Surprisingly, a recent experiment²⁴ observed that Li-Sn eutectic has a smaller retention ratio of D than pure Sn against intuition. Although the above experiment may suffer from contaminants such as oxygen and carbon at the surface of the sample, it is still worth understanding the fundamental processes regarding the interactions of hydrogen isotopes with liquid Li-Sn. For example, how do D atoms escape from Li-Sn eutectic, causing the low retention ratio of D in Li-Sn? More importantly, what is the underlying mechanism that explain liquid Li, Sn, and Li-Sn interact differently with D?

In this work, we performed first-principles molecular dynamics (FPMD) simulations to tackle the above issues. We observe the formation and evaporation of D_2 molecules in the Li-Sn slab, which may be a reason for the low retention ratio of D observed in experiment.²⁴ These results are remarkable, because as predicted by recent FPMD studies, D_2 molecules hardly form in liquid Li because D atoms form strong ionic bonds with Li atom,²⁹ whereas forming D_2 molecules is also difficult in liquid Sn, which may be caused by the low reactivity of D in liquid Sn.³⁰ In addition, it is still inconclusive which molecules can escape the surfaces of Li-Sn slab.

Very recently, an independent work³¹ has also found the formation of D_2 molecules and D_2 bubbles in bulk liquid Li-Sn systems with FPMD simulations. However, the detailed forming processes of D_2 molecules have not been fully explored. Furthermore, due to the lack of vacuum in the study, the evaporation of molecules was not investigated. Herein, we prepare two Li-Sn slabs with low and high concentrations of D atoms. We unveil a cooperative mechanism of forming D_2 molecules in liquid Li-Sn slabs, where Li atoms play a central role to trap a D atom, and wait for a second D to come nearby, triggering the forming process of D_2 molecule. During the formation of D_2 molecule, the surplus electrons are transferred from D_2 to its adjacent Sn atoms. D_2 molecules then diffuse rapidly by leaving their adjacent Li and Sn atoms. Importantly, in the low concentration case, we find the existence of both D_2 molecules and LiD molecules in the vacuum area of the simulated cell. Our results show that LiD molecules are more difficult to form than D_2 molecules below 873 K, and we predict a optimal temperature window in the low concentration case that allows evaporation of D_2 molecules from surfaces of PFCs but not for LiD molecules,

which may potentially contaminate the plasma. The above findings offer a series of new microscopic insights into our understanding of how hydrogen isotopes interact with liquid Li-Sn eutectic.

II. COMPUTATIONAL DETAILS

All of the FPMD simulations were performed with the ABACUS (Atomic-orbital Based Ab-initio Computation at USTC) package.³⁶ We adopted norm-conserving pseudopotentials³⁷ and local density approximation.³⁸ We chose an energy cutoff of 120 Ry for charge density and only the gamma point to sample the Brillouin zone with periodic boundary conditions. We used numerical atomic orbitals³⁹ as basis sets to construct the electronic wave functions. Specifically, double-zeta plus polarized (DZP) orbital sets were adopted for D ($2s1p$), Li ($2s1p$) and Sn ($2s2p1d$).^{39,40} The radius cutoffs of numerical atomic orbitals were chosen to be 6.0, 9.0 and 8.0 bohr for D, Li, and Sn elements, respectively. Born-Oppenheimer molecular dynamics simulations were performed in the canonical ensemble NVT with the Nosé-Hoover thermostat^{41,42} at 573, 673, and 873 K. A liquid Li-Sn slab with a vacuum and two concentrations of D atoms in a periodic cell ($60 \times 14.98 \times 14.98 \text{ \AA}^3$ where the vacuum is placed along x -axis) was studied. A $\text{Li}_{0.19}\text{Sn}_{0.76}\text{D}_{0.05}$ slab containing 36 Li, 144 Sn, and 10 D atoms is referred as the low concentration system, while a $\text{Li}_{0.13}\text{Sn}_{0.51}\text{D}_{0.36}$ slab consisting of 36 Li, 144 Sn, and 100 D atoms is referred as the high concentration system for brevity. We performed FPMD simulations with 30 ps trajectories for the $\text{Li}_{0.19}\text{Sn}_{0.76}\text{D}_{0.05}$ slab at temperatures of 573, 673, and 873 K. In addition, we ran FPMD simulations with 20, 24, and 22 ps trajectories for the $\text{Li}_{0.13}\text{Sn}_{0.51}\text{D}_{0.36}$ slab at temperatures of 573, 673, and 873 K, respectively. For comparison, we also carried out FPMD simulations for bulk $\text{Li}_{0.2}\text{Sn}_{0.8}$ (36 Li and 144 Sn atoms) and $\text{Li}_{0.19}\text{Sn}_{0.76}\text{D}_{0.05}$ (36 Li, 144 Sn, and 10 D atoms) systems. The ionic densities of the two bulk systems were obtained by performing FPMD simulations in the NVT ensemble with varying cell volumes until the averaged pressure is less than 1 GPa; the resulting cell sizes of the bulk $\text{Li}_{0.2}\text{Sn}_{0.8}$ and $\text{Li}_{0.19}\text{Sn}_{0.76}\text{D}_{0.05}$ systems are $23.14 \times 14.20 \times 14.20 \text{ \AA}^3$ and $23.01 \times 14.12 \times 14.12 \text{ \AA}^3$, respectively. We generated 20 ps trajectories for the two systems. The time step of FPMD simulations utilized in systems with D atoms was set to 0.2 fs to better characterize the D atoms that have a small mass; for those Li-Sn systems without D

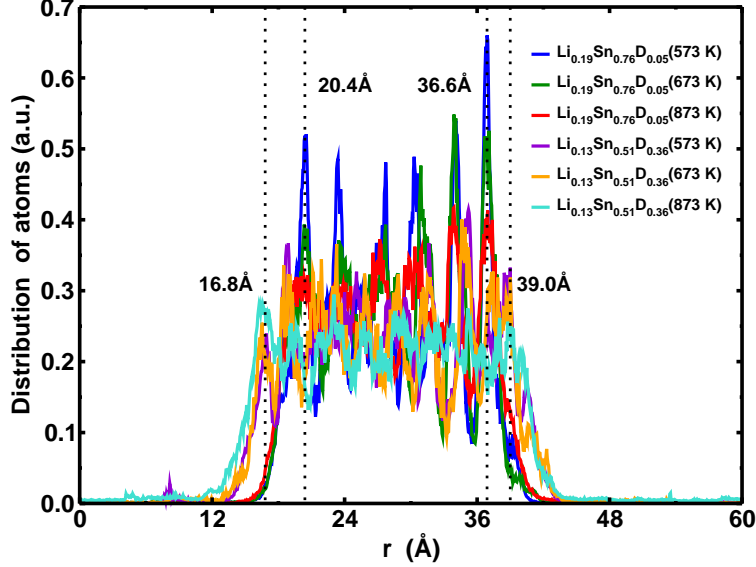


FIG. 1: (Color online) Ionic density profiles of the $\text{Li}_{0.19}\text{Sn}_{0.76}\text{D}_{0.05}$ and $\text{Li}_{0.13}\text{Sn}_{0.51}\text{D}_{0.36}$ slabs along the surface normal direction at 573, 673, and 873 K. The two dashed lines at 20.4 and 36.6 Å represent the surfaces of the $\text{Li}_{0.19}\text{Sn}_{0.76}\text{D}_{0.05}$ Li-Sn slab, while the other two dashed lines at 16.8 and 39.0 Å indicate the surfaces of the $\text{Li}_{0.13}\text{Sn}_{0.51}\text{D}_{0.36}$ Li-Sn slab.

atoms, the time step was set to 0.5 fs.

The liquid configurations of Li-Sn slabs were generated by performing FPMD simulations as follows. We first ran FPMD simulations of a $\text{Li}_{0.20}\text{Sn}_{0.80}$ slab for 5.0 ps at 1073 K with a time step of 0.5 fs in order to obtain its liquid structure. Next, we randomly inserted 10 and 100 deuterium (D) atoms into the $\text{Li}_{0.20}\text{Sn}_{0.80}$ system to generate two systems with different D concentrations, i.e., $\text{Li}_{0.19}\text{Sn}_{0.76}\text{D}_{0.05}$ and $\text{Li}_{0.13}\text{Sn}_{0.51}\text{D}_{0.36}$ systems, respectively. We then ran FPMD simulations at selected temperatures, i.e., 573, 673 and 873 K. The lengths of the trajectories have been described above. In order to let the systems evolve towards the equilibrium state, our analysis was based on the last 20 ps trajectories.

III. RESULTS AND DISCUSSIONS

A. Li-Sn Surfaces

Figure 1 illustrates the simulated ionic density profiles of liquid Li-Sn systems with both low and high concentrations of D atoms at 573, 673, and 873 K. We can see that the

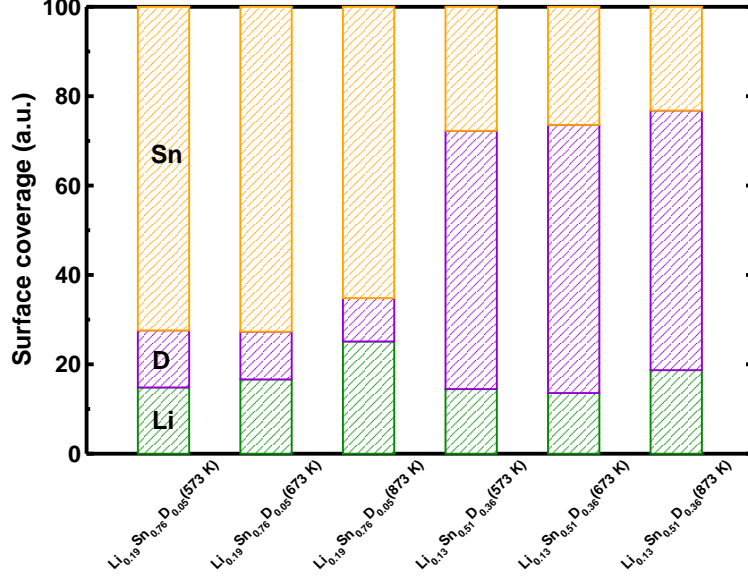


FIG. 2: (Color online) Surface coverages of Li, Sn, and D atoms in the $\text{Li}_{0.19}\text{Sn}_{0.76}\text{D}_{0.05}$ and $\text{Li}_{0.13}\text{Sn}_{0.51}\text{D}_{0.36}$ slabs at 573, 673, and 873 K.

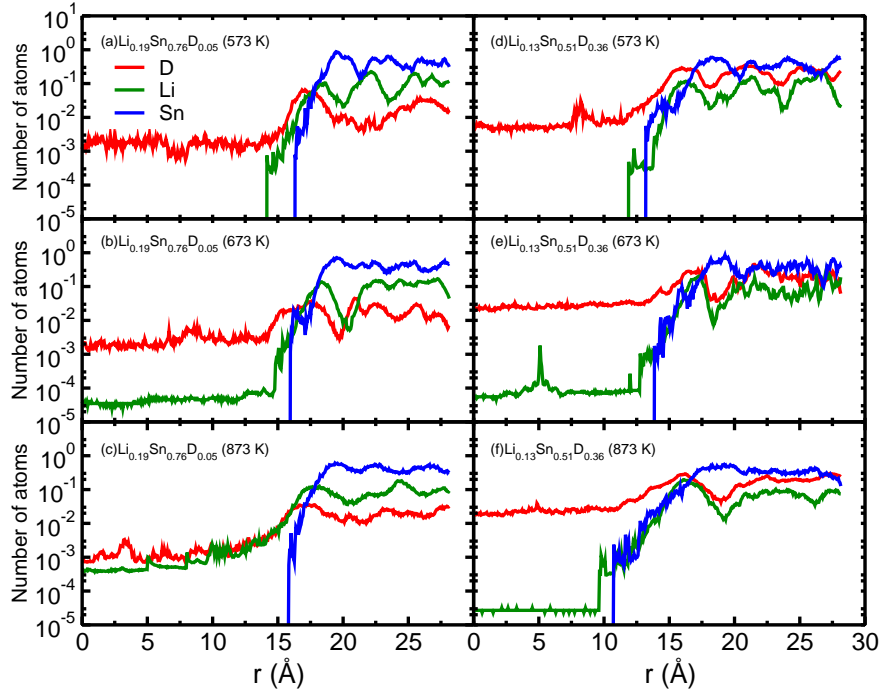


FIG. 3: (Color online) Counted number of atoms per snapshot of D, Li, and Sn atoms along the surface normal direction r of the $\text{Li}_{0.19}\text{Sn}_{0.76}\text{D}_{0.05}$ and $\text{Li}_{0.13}\text{Sn}_{0.51}\text{D}_{0.36}$ slab systems. The density profiles are averaged over the two surfaces. The interval of r is chosen to be 0.06 \AA .

volume of a Li-Sn slab is insensitive to temperatures ranging from 573 to 873 K. This is due to the fact that Li-Sn eutectic is a metallic liquid, whose volume increases by about 1% per 100 degrees. For temperature that increases from 573 to 873 K, the length of the slab along the surface normal direction (x direction) slightly changes. Therefore, we define the surface of a Li-Sn slab as the space between the first peak of the ionic density profile and the vacuum as shown in Figure 1, while the bulk of the slab is defined as the space between the two surfaces of the slab. Since the volume of a Li-Sn-D slab is insensitive to temperatures, we take the Li-Sn-D slab systems at 673 K to define the bulk region of the slab. Specifically, we define the bulk region of the $\text{Li}_{0.19}\text{Sn}_{0.76}\text{D}_{0.05}$ slab system as the space ranging from $x=20.4$ to 36.6 Å as shown in Figure 1. In addition, the volume of the Li-Sn-D slab substantially increases with a higher concentration of D. In this regard, the bulk region of the $\text{Li}_{0.13}\text{Sn}_{0.51}\text{D}_{0.36}$ slab system is defined as the space covering from $x=16.8$ to 39.0 Å. We also observe that the ionic density profiles of Li-Sn systems exhibit a series of sharp peaks, which may be due to the finite size effects. However, the heights of peaks decrease at higher temperatures, suggesting a more uniform distribution of atoms in the slabs at higher temperatures. We also compute the mean square displacements (MSD) of Li and Sn atoms in both low- and high-concentration systems at 573 K and found the increase of MSD with respect to time (see Supplementary Materials), suggesting that atoms are in the liquid state.

Figure 2 shows the surface compositions of Li-Sn-D slabs from simulations. For both Li-Sn-D systems, we observe a similar trend as compared to experiment²⁰⁻²² that the surface coverage of Li increases at a higher temperature, which can be explained as Li reduces the surface tension more effectively than Sn.^{20,23} In addition, the surface coverage of D only slightly decreases with increasing temperature; however, in the high-concentration Li-Sn system, the surface coverage of D is twice more than that of Sn, although the total number of Sn atoms is slightly larger than the number of D atoms.

Figure 3 illustrates the density profiles of Li-Sn-D slab systems decomposed into atomic components. Both low- and high-concentration slab systems at temperatures of 573, 673, and 873 K are considered. We average two surfaces of a slab in order to yield more converged results. We find that the outmost surface areas are dominated by Li atoms rather than Sn atoms in all of the six systems shown in Figure 3, which suggests that Li atoms are segregated to the surface of the Li-Sn-D slab system.

However, since the FPMD simulations are extremely expensive, the lengths of our FPMD trajectories are limited to a few tens of ps and the system only consists of a few hundred atoms. It would be possible that the segregation of Li to the surface is faster in a short time scale because the velocities of Li atoms are higher and the system has not yet reached the equilibrium state. Additionally, the sharp peaks also imply that the trajectory length may not be long enough to smooth out the inherent ordering in the Li-Sn-D slabs. In order to obtain a thorough understanding of the segregation effect and the density profiles in the Li-Sn slab systems, substantially larger systems with much longer trajectories in MD simulations are needed in future works. However, we consider the FPMD trajectories are still meaningful to yield important properties of D, such as the formation and evaporation of D_2 molecules and LiD molecules at the Li-Sn surfaces.

B. Formation of D_2 Molecules

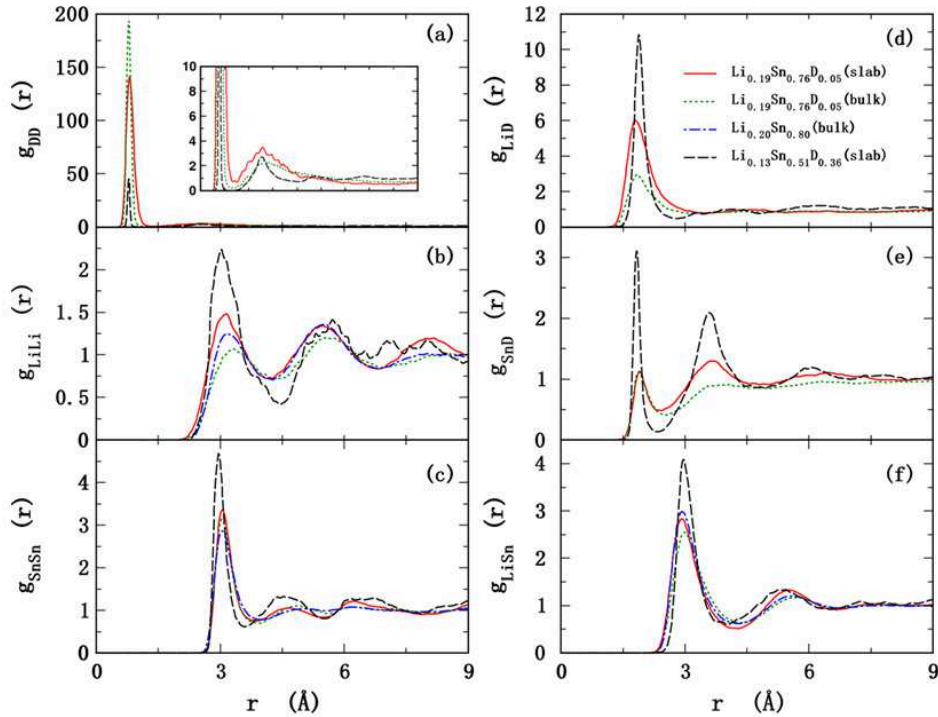


FIG. 4: (Color online) Partial pair distribution functions of (a) D-D, (b) Li-Li, (c) Sn-Sn, (d) Li-D, (e) Sn-D, (f) Li-Sn in the $Li_{0.19}Sn_{0.76}D_{0.05}$ slab (red lines), the $Li_{0.19}Sn_{0.76}D_{0.05}$ bulk (green lines), the $Li_{0.20}Sn_{0.80}$ bulk (blue lines), and the $Li_{0.13}Sn_{0.51}D_{0.36}$ slab (black lines) at 673 K.

Figure 4 illustrates the partial pair distribution functions $g_{\alpha\beta}(r)$ of D-D, Li-Li, Sn-Sn, Li-D, Sn-D, and Li-Sn, which were obtained with FPMD simulations in the liquid $\text{Li}_{0.19}\text{Sn}_{0.76}\text{D}_{0.05}$ and $\text{Li}_{0.13}\text{Sn}_{0.56}\text{D}_{0.36}$ slabs at 673 K. As comparisons, we also show the pair distribution functions for bulk $\text{Li}_{0.20}\text{Sn}_{0.80}$ and $\text{Li}_{0.19}\text{Sn}_{0.76}\text{D}_{0.05}$ systems.

The partial pair distribution function $g_{\alpha\beta}(r)$ with two different atomic species α and β is defined as

$$g_{\alpha\beta}(r) = \frac{N_{\alpha} + N_{\beta}}{\rho N_{\alpha} N_{\beta}} \sum_{i=1}^{N_{\alpha}} \sum_{j=1}^{N_{\beta}} \langle \delta(\mathbf{r} + \mathbf{R}_i - \mathbf{R}_j) \rangle, \quad (1)$$

where ρ is the atomic density, N_{α} and N_{β} are the numbers of atoms for species α and β , respectively. \mathbf{R}_i and \mathbf{R}_j are the atomic positions of atoms i and j . The above formula can be directly applied to bulk systems. For a slab system, we only compute $g_{\alpha\beta}(r)$ for the bulk region of the slab, which has been defined above. First of all, we can see that the partial pair distribution functions in Figures 4(b-f) all exhibit liquid-like structural characteristics. As can be seen from Figure 4(a), $g_{DD}(r)$ with peaks centered at around 0.8 Å suggests that D_2 molecules form in the liquid $\text{Li}_{0.19}\text{Sn}_{0.76}\text{D}_{0.05}$ slab and bulk, as the typical bond length of a D_2 molecule is 0.74 Å. Both in the bulk and in the slab, the Li-D pair distribution functions have strong peaks around 1.85 Å, suggesting that Li-D may form strong bonds. We can see that most partial pair distribution functions from the high-concentration slab system exhibit more prominent peaks. The result indicates that the $\text{Li}_{0.13}\text{Sn}_{0.51}\text{D}_{0.36}$ slab system is more structured as compared to the $\text{Li}_{0.19}\text{Sn}_{0.76}\text{D}_{0.05}$ slab system, which may be caused by the presence of high-concentration D atoms in the system. Besides, the result also implies that Li and Sn atoms in the high-concentration slab system interact more strongly with D atoms than those in the low-concentration slab system.

In the analyzed 20-ps FPMD trajectories of the $\text{Li}_{0.19}\text{Sn}_{0.76}\text{D}_{0.05}$ slab, we observe 6, 8, and 6 stable formation events of D_2 molecules at 573, 673, and 873 K, respectively. Among the formation events, 4, 3, and 5 D_2 molecules respectively evaporate into the vacuum in the system at 573, 673, and 873 K, whereas others only diffuse in the bulk region. We show two examples in the $\text{Li}_{0.19}\text{Sn}_{0.76}\text{D}_{0.05}$ slab system in Figure 5, where we record the period from the formation of a D_2 molecule to the decomposition of a D_2 molecules into two D atoms. From this figure, we observe oscillations of the bond length of two D_2 molecules; one in the vacuum and the other in the slab near the surface. In Figure 5(a), a D_2 molecule evaporates into the vacuum at around 11.14 ps and then redeposits into another surface of the slab

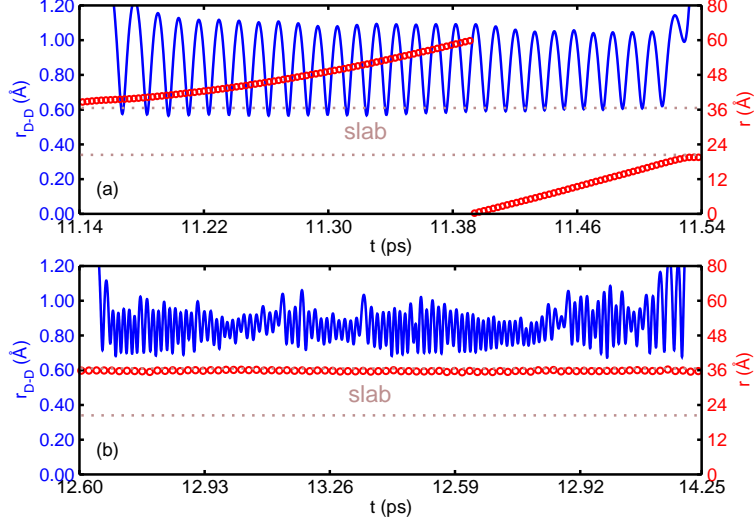


FIG. 5: (Color online) Two stable formation events of D_2 molecules in the $Li_{0.19}Sn_{0.76}D_{0.05}$ slab system. The cell length along the surface normal direction r is 60 Å. For convenience, we plot $r = 60$ to 80 Å in order to see the oscillations of the bond length r_{D-D} of a D_2 molecule. Periodic boundary conditions are used.

at about 11.54 ps. In Figure 5(b), a D_2 molecule forms at the surface at about 12.60 ps and decomposes to D atoms at around 14.25 ps. Due to the periodic boundary conditions, most of the D_2 molecules that evaporate into the vacuum redeposit into the other surface of the slab. The number of D_2 molecules observed in the vacuum is therefore smaller than the number of evaporation events, as shown in Figure 6(a). In contrast, we find several D_2 molecules that exist in the vacuum of the $Li_{0.13}Sn_{0.51}D_{0.36}$ system, and D clusters only exist in the bulk region, as illustrated in Figure 6(b). This can be explained as the D atoms are saturated in the high-concentration slab system, so more D_2 molecules evaporate to the vacuum. Furthermore, we do not observe evaporation of single D atoms or D clusters in the high-concentration case.

During the preparation of Li-Sn-D samples, each D atom was randomly implanted in the liquid Li-Sn slab before the simulations. Hence, D_2 molecules can only form from individual D atoms in the Li-Sn sample during the simulations,³¹ and then escape into the vacuum area of the simulation cell. In addition, D_2 molecules are only found to dissociate into D atoms inside the Li-Sn slab but not in the vacuum. The evaporation of D_2 molecules instead of D atoms or D clusters in both low and high concentrations of Li-Sn-D systems provides some clues to the recent experiment.²⁴ A very recent work has also found the formation of

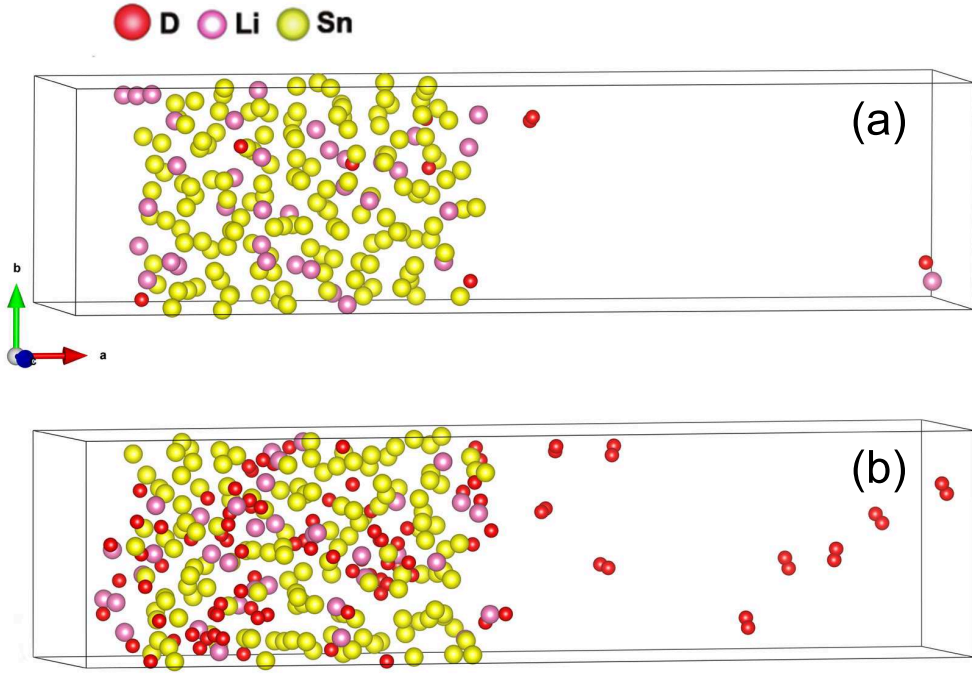


FIG. 6: (Color online) Representative snapshots of (a) $\text{Li}_{0.19}\text{Sn}_{0.76}\text{D}_{0.05}$ slab system at 873 K and (b) $\text{Li}_{0.13}\text{Sn}_{0.51}\text{D}_{0.36}$ slab system at 673 K from first-principles molecular dynamics. The Li, Sn and D atoms are labeled with pink, yellow and red colors, respectively.

D_2 molecules in bulk liquid Li-Sn systems with FPMD simulations.³¹ However, due to the limitations of the FPMD simulations that trajectories are still too short, it is very difficult to compare even quantitatively the calculated percentage of released D_2 molecules with the experiments, where almost all D_2 molecules are released.²⁴ Additionally, several factors that exist in experiments but are not considered in our simulations. For example, in the experiments, the liquid slabs may not be in the equilibrium state due to the continuous bombardments of deuterium atoms and the defects in the slab may also affect the final results. However, by investigating the 20 stable formation events of D_2 molecules from the low concentration case at temperatures of 573, 673, and 873 K, we analyze the detailed forming processes of D_2 molecules. We do not investigate the formation of D_2 molecules in the high-concentration case because a large number of D atoms exist in the slab, some of which form D clusters. Therefore, it is challenging to have an algorithm to define D_2 molecules in D clusters. In addition, even if we can identify D_2 molecules in the high-

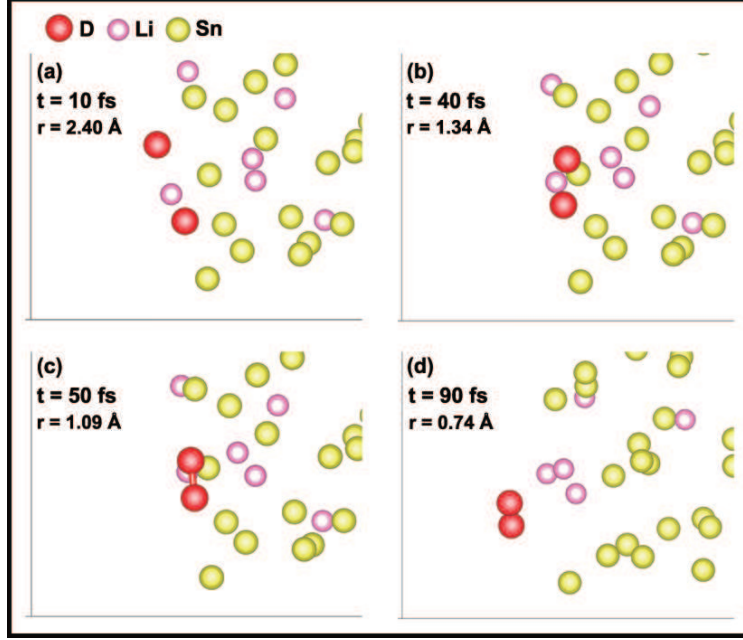


FIG. 7: (Color online) A series of steps to form D_2 molecules in the $Li_{0.19}Sn_{0.76}D_{0.05}$ slab at 673 K. (a) Li and Sn trap a D atom at the surface. (b) Two D atoms come closer at the surface. (c) Formation of a D_2 molecule. (d) The D_2 molecule diffuses away from Li and Sn atoms. t is the simulation time, whereas r is the distance between the two D atoms.

concentration case, it is still difficult to get a clear picture about how D atoms interact with Li and Sn atoms before a D_2 molecule forms, because the existence of adjacent D atoms complicates the analysis. In contrast, in the low-concentration case, the generation of each D_2 molecule can be nonambiguously identified and the forming process can be analyzed. More importantly, the low-concentration case is a more realistic case in a fusion device that uses liquid metals as shields because huge amounts of D atoms bombarding liquid wall is unlikely to occur in an operating fusion device.

In a previous FPMD simulation work of inserted D atoms in bulk Li,²⁹ the formation of D_2 molecules did not occur when the proportion of D atoms is smaller than that of Li atoms due to the strong bonding between Li and D atoms. Only a small amount of D_2 molecules were recorded when the proportions of D and Li are equal. In another FPMD simulation work, no D_2 formation with a long lifetime was observed in pure liquid Sn.³⁰ In stark contrast, in the Li-Sn slab, a considerable number of D_2 molecules form in a system with more Li than D, indicating there may be a different mechanism to form D_2 in the Li-Sn

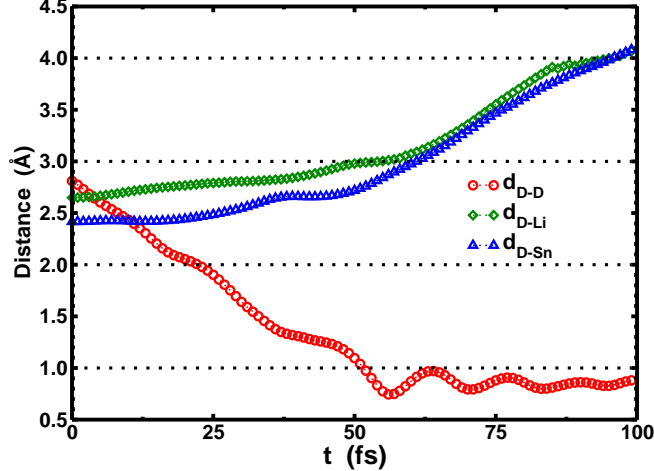


FIG. 8: (Color online) Distances from D atoms to its adjacent atoms in the $\text{Li}_{0.19}\text{Sn}_{0.76}\text{D}_{0.05}$ slab during the formation of D_2 molecules. $d_{\text{D-D}}$, $d_{\text{D-Li}}$, and $d_{\text{D-Sn}}$ are defined as the distances between D and its adjacent D, Li, and Sn atoms, respectively. The results are averaged over 20 stable formation events of D_2 molecules found in the $\text{Li}_{0.19}\text{Sn}_{0.76}\text{D}_{0.05}$ slab at temperatures of 573, 673, and 873 K.

eutectic. Based on our analysis, there are typically four steps to form D_2 molecules in the Li-Sn slab as shown in Figure 7 (see the movie in the SM)⁴³: In the first step, a D atom is first trapped by a Li atom in the Li-Sn slab to form a Li-D pair, as shown in Figure 7(a). The trapped D keeps moving at a relatively low velocity, setting up a stable environment with adjacent Li and Sn atoms and waiting for other D atoms to form a D_2 molecule. Figure 4(a) further demonstrates that D atoms interact strongly with Li atoms, as can be seen by the high first peak of $g_{\text{LiD}}(r)$. Next, Figure 7(b) shows that a second D atom comes close to the first D, while the position of the Li-D pair does not change much. As will be explained later, we find that the second D atom slows down and diffuses towards the first D. Third, a D_2 molecule starts to form by triggering the charge transfer from D to its adjacent Sn atoms (*vide infra*), as shown in Figure 7(c). In the last step, the newly formed D_2 molecule diffuses away from its Li and Sn neighbors as illustrated in Figure 7(d). We also provide a movie⁴³ that shows the formation of a D_2 molecule near the surface of $\text{Li}_{0.19}\text{Sn}_{0.76}\text{D}_{0.05}$ system (673 K) and evaporation of this D_2 molecule into the vacuum (see the Supporting Information).

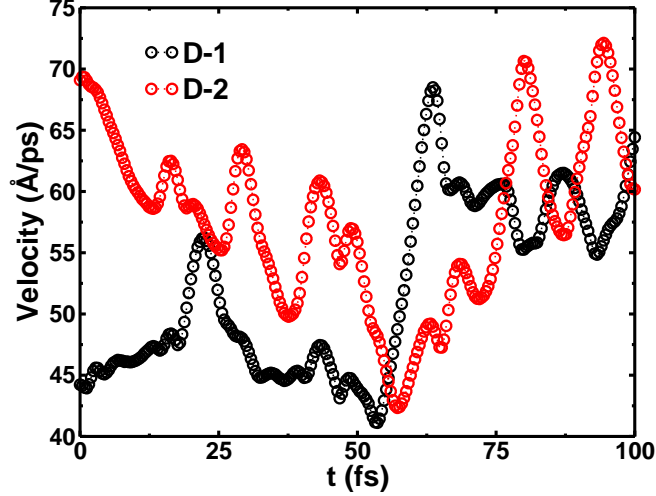


FIG. 9: (Color online) Velocities of two D atoms (labeled as D-1 and D-2) during the formation of D_2 molecules in the $Li_{0.19}Sn_{0.76}D_{0.05}$ slab. The results are averaged over 20 stable formation events of D_2 molecules found in the $Li_{0.19}Sn_{0.76}D_{0.05}$ slab at temperatures of 573, 673, and 873 K.

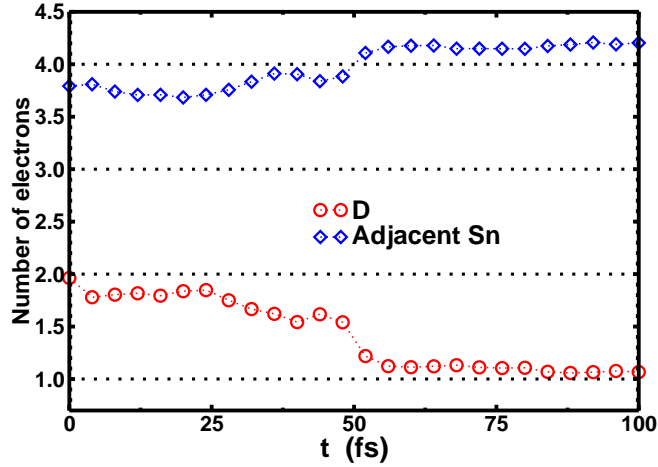


FIG. 10: (Color online) Number of electrons on D and its adjacent Sn atoms during the formation of a D_2 molecule in the $Li_{0.19}Sn_{0.76}D_{0.05}$ slab. The results are averaged over 20 stable formation events of D_2 molecules found in the $Li_{0.19}Sn_{0.76}D_{0.05}$ slab at temperatures of 573, 673, and 873 K.

C. Processes of Forming D_2

We systematically analyze the processes of forming D_2 molecules in order to quantify the above observations in simulations. For those properties illustrated in Figure 8, Figure 9, and Figure 10, we average 20 stable formation events of D_2 molecules. The 20 events are collected from the 6, 8, and 6 stable formation events of D_2 in the low-concentration system at

temperatures of 573, 673, and 873 K, respectively. Although more stable formation events of D_2 molecules are expected at higher temperatures, it is counter intuitive that only 6 events of D_2 are found at 873 K, which is smaller than the 8 events of D_2 found at 673 K. Nevertheless, at 873 K, we record 10 evaporation events of LiD molecules (*vide infra*), indicating that some of the D atoms in the low-concentration slab system are involved in forming LiD molecules.

In particular, we track the D-D pairs in the low-concentration Li-Sn slab and report their interesting dynamics. The criterion to track D-D pairs was selected when any two D atoms come close within 1.1 Å and last for more than 0.2 ps. Moreover, we chose a time window of 100 fs that is relevant to the formation of D_2 molecules, emphasizing the formation moment which occurs at around 50 fs corresponding to Figures 7(a-c). By investigating the changes of properties before and after the formation of D_2 molecules within the 100 fs, we can obtain insights into the fundamental process of forming D_2 molecules. Specifically, the analyzed time-dependent properties include distances of D to its neighbors, instantaneous velocities of D atoms, and number of electrons on D, which are respectively shown in Figure 8, Figure 9, and Figure 10, respectively. We point out that due to the limited size of systems utilized in our FPMD simulations, the structural and dynamical properties of atoms in the slab could be affected. However, in our analysis of these time-dependent properties, we only focus on a local environment around the two D atoms that form a D_2 molecule. Therefore, we expect that the size effects are not substantial in affecting these properties. In addition, the number of D atoms in the low-concentration system is only 10 due to the limited size of the system, we observe 20 stable formation events of D_2 molecules from 573, 673, and 873 K. Although the current work could not provide more detailed temperature-dependent forming mechanisms for D_2 molecules, we still consider the averaged properties from the 20 events are sufficient to provide useful information.

Figure 8 shows that the distance between two D atoms (d_{D-D}) quickly shortens approximately from 2.8 to 0.8 Å in the first 50 fs before the formation of D_2 , and then stably oscillates around 0.8 Å with a damped amplitude up to 100 fs. The value of 0.8 Å is the location of the first peak of the partial pair distribution function $g_{DD}(r)$, as illustrated in Figure 4(a). Meanwhile, the distances between D atoms and its adjacent atoms, i.e., d_{D-Li} and d_{D-Sn} , slowly elongates from around 2.5 to 2.8 Å during the first 50 fs, which can be understood since Li and Sn atoms should provide spaces for two neighboring D atoms to meet and the process of forming D_2 starts. Meanwhile, as displayed in Figures 4(d) and (e),

D atoms start to deviate from positions of the first peak in $g_{\text{LiD}}(r)$ and $g_{\text{SnD}}(r)$, indicating that the interactions between D and Li/Sn atoms are weakened. We then see a dramatic increase of $d_{\text{D-Li}}$ and $d_{\text{D-Sn}}$ from around 2.8 to 4.0 Å within the second 50 fs, suggesting that the D_2 molecule quickly diffuses away after its formation (see Figure 7(d) and the movie in the Supplementary Materials).⁴³

The averaged velocities of the selected D-D pairs during the formation of D_2 molecules are illustrated in Figure 9. One of the two D atoms (labeled as D-1) has a velocity that is slower than the velocity of the other D atom (labeled as D-2) in the first 50 fs, indicating that the two D atoms are experiencing different environments, i.e., the D-1 atom is trapped by surrounding Li and Sn atoms and the D-2 atom diffuses freely in the liquid with its velocity abruptly drops. During the formation of D_2 molecule at around 50 fs, the two D atoms slow down and we know from Figure 8 that a bond forms between them. Next, after the formation of a D_2 molecule, both D-1 and D-2 atoms experience a vast increase of velocity after the 50 ps, and then diffuse together with similar velocities.

In Figure 10, we also compute the averaged charge change of D atoms and their adjacent atoms during the formation of D_2 molecules. We utilized the Bader charge analysis method.⁴⁴ From this analysis, we find electrons transfer from D to Sn atoms during the formation of D_2 molecules. Quantitatively, before forming D_2 molecules at around 50 fs, more than 1.5 electrons are assigned to a D atom while less than 4.0 valence electrons per atom are on its nearby Sn atoms. In the first 50 fs, a small amount of electrons (less than 0.5 electrons per atom) on D transfer to Sn. When D_2 forms at around 50 fs, the number of electrons on the D atom abruptly drops to about 1.0 within a very short time, which occurs at the same time when the changes of distances and velocities of D atoms occur. Meanwhile, the electrons on Sn are accumulated to above 4.0. The resulting number of electrons on D is slightly above 1.0, which is close to that of a single D atom. Furthermore, the D-D pair therefore has a bond of around 0.8 Å with two electrons. Therefore, we identify the formation of D_2 molecules in the liquid Li-Sn slab based on all of the above considerations. It should be noted that no electrons are assigned to Li according to the Bader analysis, suggesting Li loses all its 2s valence electrons in the metallic liquid Li-Sn slab.

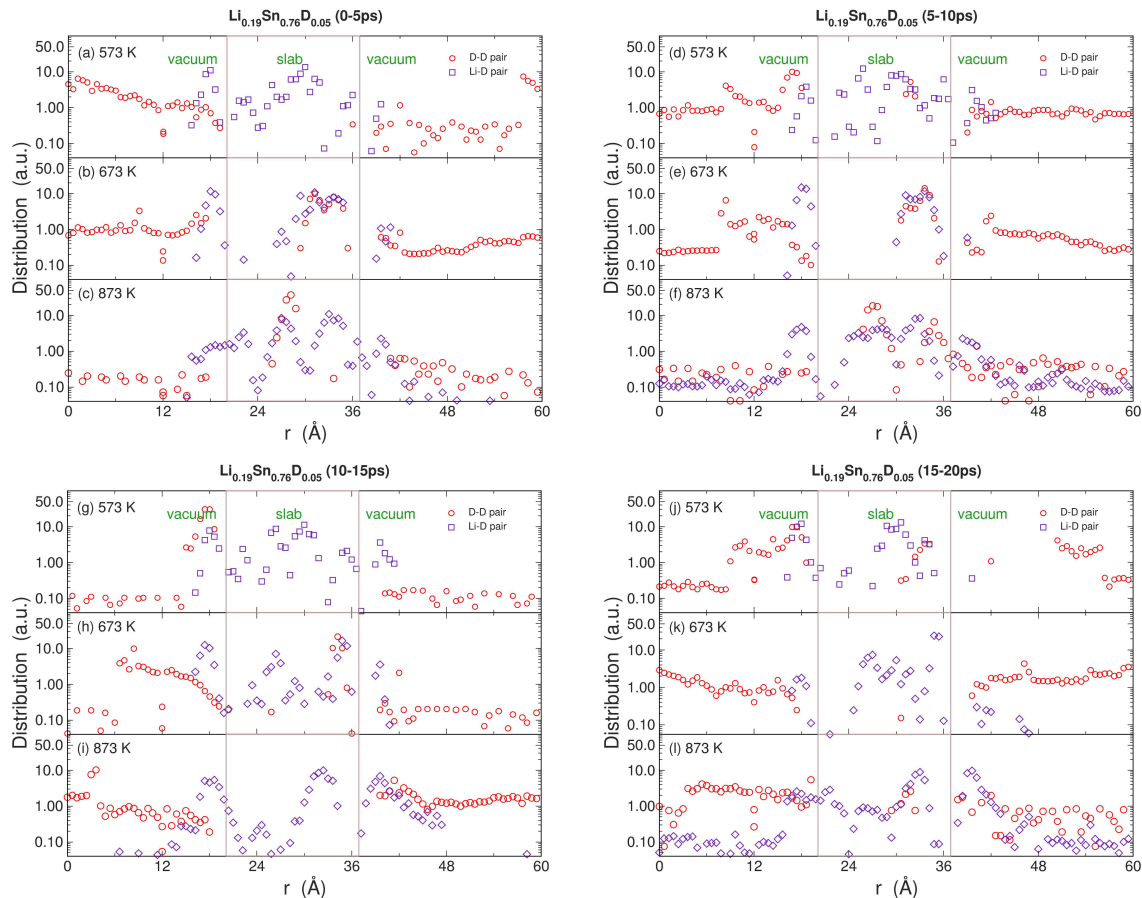


FIG. 11: (Color online) Distributions of D-D and Li-D pairs in the $\text{Li}_{0.19}\text{Sn}_{0.76}\text{D}_{0.05}$ slab system along the surface normal direction at 573, 673 and 873 K. Distributions of D-D and Li-D pairs are divided into four parts according to the length of trajectories, i.e., (a-c) 0-5, (d-f) 5-10, (g-i) 10-15, (j-l) 15-20 ps. The region within the two solid brown lines is defined as the bulk of Li-Sn.

D. Formation of LiD Molecules

The FPMD simulations show that the D_2 molecules diffuse rapidly in the Li-Sn eutectic and some of them evaporate into the vacuum. Although we observe no evaporation of single D atoms or Li_2 molecules in liquid Li-Sn slab systems from the FPMD trajectories, we find the existence of LiD molecules in vacuum, which is not surprising since Li and D atoms form strong ionic bonds and tend to stay near the surface. To be specific, we observe 10 evaporation events for LiD molecules in the low-concentration slab system at 873 K, while only 1 evaporation event of LiD molecules is found in the high-concentration slab system at 673 K. Additionally, according to the clues provided by the atomic decomposed density

profiles illustrated in Figure 3, we respectively observe 2 and 1 events for a single Li atom that appears in the vacuum region of the low- and high-concentration slab systems at 873 K. Based on the above findings, we focus on discussing the formation of LiD molecules in the low-concentration slab system at 873 K since more evaporation cases are observed in this system than those in other systems.

Because Li could potentially contaminate the plasma, it is important to know how the LiD molecules evaporate compared to D_2 . Figure 11 depicts the distributions of D_2 and LiD molecules in the low-concentration Li-Sn slab at 573, 673, and 873 K. We divide the 20 ps trajectory into four parts, i.e., 0-5, 5-10, 10-15, 15-20 ps. D_2 molecules distribute in both liquid Li-Sn slab and vacuum at all temperatures considered. In contrast, Li-D pairs mostly reside in the Li-Sn slab at 573 and 673 K, and are occasionally recorded around the surface. At the higher temperature of 873 K, we find a small amount of LiD molecules escape to the vacuum, although the chance to find the LiD molecules is almost an order of magnitude smaller than that of D_2 molecules. This finding is significant, because it suggests that the facility should work in an optimal temperature window below 873 K, which allows efficient recycling of D atoms but reduce the risk of LiD molecules from contaminating the plasma.

IV. CONCLUSIONS

To summarize, we carry out FPMD simulations to investigate the retention and recycling of deuterium in liquid Li-Sn with two different concentrations ($Li_{0.19}Sn_{0.76}D_{0.05}$ and $Li_{0.13}Sn_{0.51}D_{0.36}$) at three temperatures of 573, 673, and 873 K. First of all, we find the formation of D_2 molecules in all of the simulations. Importantly, we unveil a cooperative mechanism of forming D_2 molecules in liquid Li-Sn, where Li atoms behave as catalytic centers, allowing efficient generation of D_2 molecules in liquid metal Li-Sn. During the formation process, Li traps a D atoms and another D atom comes close to trigger the charge transfer from D atoms to their nearby Sn atoms. After formation, the D_2 molecules diffuse promptly in the Li-Sn liquid and evaporate to the vacuum. The above mechanism reduces the retention of D in liquid Li-Sn slabs, and is beneficial for the recycling of D atoms. This work therefore provides new clues to a recent experimental finding²⁴ that Li-Sn eutectic has an unexpected low retention rate of hydrogen isotopes. Furthermore, although we do not observe evaporation of single D atoms or Li_2 molecules in our simulations, we

occasionally observe the evaporation of LiD molecules in the high-concentration slab system at 673 K and the appearance of Li atoms in the vacuum in both concentrations of systems at 873 K. Importantly, we observe a substantial amount of LiD molecules, which form and evaporate in the low-concentration slab system at 873 K. We predict a temperature window below 873 K, allowing efficient recycling of D atoms but reduce the risk of LiD molecules from contaminating the plasma. The new findings deepen our understanding of interactions between hydrogen isotopes and liquid Li-Sn and can be potentially used for improving the design of magnetically confined fusion reactors. Because the FPMD simulations of liquid slabs are computationally very expensive, currently we can only simulate a slab with a few hundred atoms for short period of times, which unavoidably suffers from size effects. Phenomena such as segregation of Li atoms to the liquid surface⁴⁵ cannot be fully reproduced in the FPMD simulations.²⁷ Simulations on much larger systems and for a longer simulation time using reliable potentials constructed by machine learning⁴⁶ is a promising routine along this direction.

V. DATA AVAILABILITY STATEMENT

The data that support the findings of this study are available from the corresponding author upon reasonable request.

Acknowledgments

Daye Zheng and Zhen-Xiong Shen contributed equally to this work. This work was funded by the National Key Research and Development Program of China (Grants No. 2016YFB0201202), and the Chinese National Science Foundation Grant number 11774327. XR acknowledges the support of the Chinese National Science Foundation Grant No. 11574283 and 11874335. The numerical calculations have been done on the USTC HPC facilities. Part of the numerical simulations was performed on the High Performance Computing Platform of CAPT.

* Electronic address: mohanchen@pku.edu.cn

- [†] Electronic address: helx@ustc.edu.cn
- ¹ R. A. Causey, *J. Nucl. Mater.* **300**, 91 (2002).
 - ² R. Mattas, J. Allain, R. Bastasz, J. Brooks, T. Evans, A. Hassanein, S. Luckhardt, K. McCarthy, P. Mioduszewski, R. Maingi, et al., *Fusion Eng. Des.* **49**, 127 (2000).
 - ³ R, T. Majeski, D. Abrams, E. Boyle, J. Granstedt, C. Hare, R. Jacobson, T. Kaita, B. Kozub, D. LeBlanc, et al., *Phys. Plasmas* **20**, 056103 (2013).
 - ⁴ T. Abrams, M. Jaworski, R. Kaita, J. Nichols, D. Stotler, G. De Temmerman, M. van den Berg, H. van der Meiden, and T. Morgan, *J. Nucl. Mater.* **463**, 1169 (2015).
 - ⁵ T. Abrams, M. Jaworski, M. Chen, E. Carter, R. Kaita, D. Stotler, G. De Temmerman, T. Morgan, M. van den Berg, and H. van der Meiden, *Nucl. Fusion* **56**, 016022 (2015).
 - ⁶ J. Coenen, G. De Temmerman, G. Federici, V. Philipps, G. Sergienko, G. Strohmayer, A. Terra, B. Unterberg, T. Wegener, and D. Van den Bekerom, *Phys. Scr.* **2014**, 014037 (2014).
 - ⁷ B. Lipschultz, J. Coenen, H. Barnard, N. Howard, M. Reinke, D. Whyte, and G. Wright, *Nucl. Fusion* **52**, 123002 (2012).
 - ⁸ RA, S. Pitts, F. Carpentier, T. Escourbiac, V. Hirai, S. Komarov, A. Lisgo, A. Kukushkin, M. Loarte, A. Merola, et al., *J. Nucl. Mater.* **438**, S48 (2013).
 - ⁹ G. Van Eden, T. Morgan, H. Van der Meiden, J. Matejicek, T. Chraska, M. Wirtz, and G. De Temmerman, *Nucl. Fusion* **54**, 123010 (2014).
 - ¹⁰ P. Fifiis, A. Press, W. Xu, D. Andruczyk, D. Curreli, and D. Ruzic, *Fusion Eng. Des.* **89**, 2827 (2014).
 - ¹¹ K. Tritz, R. E. Bell, P. Beiersdorfer, D. Boyle, J. Clementson, M. Finkenthal, R. Kaita, T. Kozub, S. Kubota, M. Lucia, et al., *Plasma Phys. Controlled Fusion* **56**, 125014 (2014).
 - ¹² M. Ono, M. Jaworski, R. Kaita, Y. Hirooka, T. Gray, and N.-U. R. Team, *Fusion Eng. and Des.* **117**, 124 (2017).
 - ¹³ R, J. Maingi, R. Canik, D. Bell, A. Boyle, R. Diallo, S. Kaita, B. Kaye, S. LeBlanc, F. Sabbagh, et al., *Fusion Eng. and Des.* **117**, 150 (2017).
 - ¹⁴ D. P. Boyle, R. Majeski, J. C. Schmitt, C. Hansen, R. Kaita, S. Kubota, M. Lucia, and T. D. Rognlien, *Phys. Rev. Lett.* **119**, 015001 (2017).
 - ¹⁵ P. Rindt, T. Morgan, M. Jaworski, and N. L. Cardozo, *Nucl. Fusion* **58**, 104002 (2018).
 - ¹⁶ T. Morgan, D. Van den Bekerom, and G. De Temmerman, *J. Nucl. Mater.* **463**, 1256 (2015).
 - ¹⁷ G. G. van Eden, T. W. Morgan, D. U. B. Aussems, M. A. van den Berg, K. Bystrov, and

- M. C. M. van de Sanden, *Phys. Rev. Lett.* **116**, 135002 (2016).
- ¹⁸ A. E. Cremona, E. Vassallo, F. Alves, S. Causa, R. De Iuliis, G. Dond, G. Giacomini, G. Gervasini, M. Granucci, et al., *Nuclear Materials and Energy* **17**, 253 (2018).
- ¹⁹ S. Weir, M. Lipp, S. Falabella, G. Samudrala, and Y. Vohra, *J. Appl. Phys.* **111**, 123529 (2012).
- ²⁰ R. Bastasz and J. Whaley, *Fusion Eng. Des.* **72**, 111 (2004).
- ²¹ J. Allain, M. Nieto, M. Coventry, R. Stubbers, and D. Ruzic, *Fusion Eng. Des.* **72**, 93 (2004).
- ²² J. P. Allain, M. D. Coventry, and D. N. Ruzic, *Phys. Rev. B* **76**, 205434 (2007).
- ²³ V. Kvon, E. Oyarzabal, E. Zoethout, A. Martin-Rojo, T. Morgan, and F. Tabarés, *Nucl. Mater. Energy* **13**, 21 (2017).
- ²⁴ JPS, H. Loureiro, F. Fernandes, G. Tabars, C. Mazzitelli, R. Silva, E. Gomes, R. Alves, T. Mateus, H. Pereira, et al., *Nucl. Mater. Energy* **12**, 709 (2017).
- ²⁵ M. Chen, L. Hung, C. Huang, J. Xia, and E. A. Carter, *Mol. Phys.* **111**, 3448 (2013).
- ²⁶ B. G. del Rio, M. Chen, L. E. González, and E. A. Carter, *J. Chem. Phys.* **149**, 094504 (2018).
- ²⁷ G. Beatriz, E. K. de Jong, and E. A. Carter, *Nuclear Materials and Energy* **18**, 326 (2019).
- ²⁸ P. S. Krstic, J. P. Allain, C. N. Taylor, J. Dadras, S. Maeda, K. Morokuma, J. Jakowski, A. Allouche, and C. H. Skinner, *Phys. Rev. Lett.* **110**, 105001 (2013).
- ²⁹ M. Chen, T. Abrams, M. Jaworski, and E. A. Carter, *Nucl. Fusion* **56**, 016020 (2015).
- ³⁰ X. Liu, D. Zheng, X. Ren, L. He, and M. Chen, *J. Chem. Phys.* **147**, 064505 (2017).
- ³¹ G. Beatriz, G. S. Gautam, and E. A. Carter, *Nuclear Fusion* **60**, 016025 (2019).
- ³² H. Moriyama, K. Iwasaki, and Y. Ito, *J. Nucl. Mater.* **191**, 190 (1992).
- ³³ S. Fukada, M. Kinoshita, K. Kuroki, and T. Muroga, *J. Nucl. Mater.* **346**, 293 (2005).
- ³⁴ T. Kulsartov, I. Tazhibayeva, Y. Ponkratov, Y. Gordienko, Z. Zaurbekova, V. Baklanov, Y. Chikhray, M. Skakov, Y. Koyanbayev, A. Korovikov, et al., *Fusion Eng. and Des.* **124**, 324 (2017).
- ³⁵ I. Tazhibayeva, Y. Ponkratov, T. Kulsartov, Y. Gordienko, M. Skakov, Z. Zaurbekova, I. Lyublinski, A. Vertkov, and G. Mazzitelli, *Fusion Eng. and Des.* **117**, 194 (2017).
- ³⁶ P. Li, X. Liu, M. Chen, P. Lin, X. Ren, L. Lin, C. Yang, and L. He, *Comput. Mater. Sci.* **112**, 503 (2016).
- ³⁷ J. P. Perdew and A. Zunger, *Phys. Rev. B* **23**, 5048 (1981).
- ³⁸ D. M. Ceperley and B. J. Alder, *Phys. Rev. Lett.* **45**, 566 (1980).
- ³⁹ M. Chen, G. Guo, and L. He, *J. Phys. :Condens. Matter* **22**, 445501 (2010).

- ⁴⁰ M. Chen, G.-C. Guo, and L. He, *J. Phys. :Condens. Matter* **23**, 325501 (2011).
- ⁴¹ S. Nose, *J. Chem. Phys.* **81**, 511 (1984).
- ⁴² W. G. Hoover, *Phys. Rev. A* **31**, 1695 (1985).
- ⁴³ (See the supplementary material at the website for more simulation details and results.).
- ⁴⁴ W. Tang, E. Sanville, and G. Henkelman, *J. Phys.: Condens. Matter* **21**, 084204 (2009).
- ⁴⁵ M. Suchoňová, J. Krištof, M. Pribula, M. Veis, F. Tabarés, and P. Veis, *Fusion Engineering and Design* **117**, 175 (2017).
- ⁴⁶ L. Zhang, J. Han, H. Wang, R. Car, and W. E, *Phys. Rev. Lett.* **120**, 143001 (2018).